Strain-Driven Moiré Superstructures of Epitaxial Graphene on Transition Metal Surfaces

Pablo Merino,[‡] Martin Švec,[‡] Anna L. Pinardi,[†] Gonzalo Otero,[†] and José A. Martín-Gago[†,‡,*]

[†]Instituto Ciencia de Materiales de Madrid-CSIC, c/. Sor Juana Inés de la Cruz, 3, 28049-Madrid, Spain, and [‡]Centro de Astrobiología, INTA-CSIC, Ctra. de Torrejon a Ajalvir, km 4, 28850 Torrejón de Ardoz, Spain

ABSTRACT STM images of multidomain epitaxial graphene on Pt(111) have been combined with a geometrical model to investigate the origin of the coincidence Moiré superstructures. We show that there is a relation between the appearance of a particular Moiré periodicity and the minimization of the absolute value of the strain between the graphene and the substrate for the different orientations between both atomic lattices. This model predicts all the stable epitaxial graphene structures that can be grown on transition metal surfaces, and we have made use of it for reproducing previously published data from different authors. Its validity suggests that minimization of the strain within the coincident graphene unit-cell due to a strong local interaction is the driving force in the formation of Moiré superstructures.

KEYWORDS: epitaxial graphene · STM · Moiré · superstructures · strain

Graphene has turned out to be the most outstanding material of the decade. Among all the different proposed applications and protocols to grow it, epitaxial graphene (EG) on single-crystal metal surfaces has acquired significant attention as a model system suitable to rationalize its atomic structure, interaction with the support, and even its excellent electronic properties.[1] Scanning tunnelling microscope (STM) images have proved the existence of Moiré superstructures in EG due to the spatial coincidence of the atomic periodicity of the graphene lattice with that of the supporting metal. Formation of Moiré superstructures has been reported on many metals, such as Ru,[2−6] Ir,[7,8] Rh,[9] Pt,[10−12] and recently Cu,[13] Pd,[14,15] Co,[16] and Ni.[17] Surprisingly, albeit the huge, recent and still increasing number of papers devoted to this topic, the most fundamental questions about the growth, structure, and stability of these Moirés have not been deeply addressed and is still a matter of scientific dispute.

The Moiré or coincidence superstructures of the EG show different periodicities and orientations for every one of the single-crystal transition metal (TM) surfaces, and usually more than one has been reported for many substrates. Thus, on Ru(0001) a Moiré cell of 12C/11Ru[4] is usually reported and a crystallographic unit cell of 25C/23Ru[2] has been found. In the case of Co(0001) a 1C/1Co structure has been described. Moreover, multiphase graphene has been reported on Ir(111), Cu(111), Ni(111), and Pd(111), where Moirés with different periodicities and angles have been characterized with different techniques.[2,8,10,11,18] This is also the case of Pt(111); the first STM investigation reported three distinct graphene superstructures with different periodicities and commented on the existence of some more.[9] Works published later[10,11,17−21] showed evidence of the existence of other additional domains. A very recent study included atomically resolved STM images of six coexisting phases.[12] The seminal works of Loginova *et al.*[8] and Sutter *et al.*[11] addressed the problem of the origin of rotational domains of graphene on TM surfaces, but they were constrained to their own experimental observations. It might seem surprising but so far the total number of periodic graphene superstructures existing on Pt(111) is still unknown. More generally, a question that has not been addressed up to now is how many Moiré superstructures can be accommodated on a particular single-crystal metal surface. It is mostly believed that EG formation is a kinetically driven process and therefore this number is unrestricted, although formation of some domains is more likely than others in terms of total energy. In this sense, DFT has shown its ability to study large unit cells for particular Moiré structures.[5,6,9] However, its use to perform a full optimization of all possible coincidence structures, looking for the most favorable rotational angles and all possible coincidences between graphene and substrate unit cells, is an unattainable

* Address correspondence to Gago@icmm.csic.es.

Received for review March 30, 2011 and accepted June 15, 2011.

Published online June 15, 2011
10.1021/nn201200j

task. We will show in this work that our geometrical model predicts the number of possible phases, and that this number is directly related to the strain minimization. The structures found by this model can be used as a starting point for complete DFT calculations or to interpret STM images.

We have addressed this topic by combining a geometrical model with STM images of multidomain EG on Pt(111). Our model predicts the formation of 22 stable superstructures for Pt(111). We have experimentally found 19 of them, which are all predicted by the model. Moreover, by applying this method to published data we can reproduce the Moiré superstructures found for other single crystal metal surfaces and we foresee the existence of periodicities that have not been yet reported. Significant conclusions regarding the stress release within the crystallographic domain induced by a strong local surface-layer interaction can be drawn out of this model.

In many of the recent reports the crystallinity of graphene layers is improved by the use of an adequate temperature for decomposition of the molecular precursor.[1] However, in this work we focus on the growth of multidomain EG, which is a very important topic because it leads to the formation of small graphene islands which may include a large number of unusual defects,[23−25] domain boundaries,[26−28] strain induced pseudomagnetic fields,[29] or exotic features, such as nanobubbles[30] and nanoribbons.[31,32] All these peculiar structures can coexist in a single preparation. The ability of STM to identify and study a particular graphene phase makes these samples to be a system where many surface science studies can be simultaneously performed. To favor the growth of multidomains in epitaxial graphene, we have used low decomposition temperatures and large polycyclic aromatic hydrocarbons (C_{60} in the present study) as molecular precursor. We have noticed that this recipe is successful in producing Moiré domains with different periodicities and angles on the same surface[22] (see Methods section for details about the multiphase growth methodology).

RESULTS AND MODEL

We have grown multidomain EG with a submonolayer coverage, and we studied its morphology and structure *in situ*, in an ultra high vacuum equipment. Figure 1 shows STM images for submonolayer coverage where several domains are imaged together with some atomically resolved clean Pt(111) regions. Graphene forms different domains with superstructures characterized by the angle between the graphene rows and the Pt [1$\bar{1}$0] surface direction. On the surface we found graphene regions with small periodicities ratio (*i.e.*, ($\sqrt{3} \times \sqrt{3}$)R30° and ($\sqrt{7} \times \sqrt{7}$)R19°) coexisting with larger Moiré superstructures. The study of hundreds of atomically resolved STM images of G/Pt(111) prepared following the recipe described in the Methods section revealed a system surprisingly rich in graphene superstructures. The low energy electron diffraction (LEED) pattern (see inset Figure 1) corroborates this finding. It shows a nonhomogeneous ring of structures at 2.4 Å, indicating that many different orientations are permitted.

Figure 2 shows some atomically resolved STM images of these graphene domains, which exhibit different angles and periodicities. Although the largest fraction of the investigated areas were covered by a ($\sqrt{7} \times \sqrt{7}$)R19° superstructure, other coincidence structures exhibiting periodicities in the range between 19 and 22 Å were often found. We will refer to these experimental structures as "large Moirés". The smallest periodicity of size 5 Å was observed occupying a fractional area about 10−15%.[22] The rest of periodicities ranging between 7.4 Å and 18 Å were found in even smaller amounts and constrained to small domains. We noticed that on the system prepared at a lower temperature (800 K) it became easier to find periodicities ranging between 7.4 and 18 Å than for the system annealed at higher temperatures (1200 K).

To describe these coincidence structures we developed a phenomenological model based on geometrical considerations. The model that we propose is illustrated in Figure 3, where the black spheres correspond to a graphene lattice lying on a single Pt layer (blue spheres) oriented with the [1$\bar{1}$0] surface direction along the horizontal axis. After superimposing both atomic networks, with a relative angle between them denoted as Φ (called from now on crystallographic angle, which in the figure is the one formed between the black-dotted line and the crystallographic [1$\bar{1}$0] direction), we observe a nearly coincidence, that is, a minimum distance between the carbon and the Pt spheres right below (enlarged in the inset at the top right of the image). The Moiré unit cell is then defined by these two orange points together with the atom at the origin (black lines); the Moiré forms another angle with the [1$\bar{1}$0] crystallographic direction that we will call Ω, the apparent angle of the Moiré. The distance between these nearly coincident points, namely the mismatch between the graphene and the substrate, is never zero, but in some cases it is very small. Thus, each Moiré superstructure can be defined by the two angles described above, Φ and Ω, and by the size of the superperiodicity, *L*, associated with it. It is worth noting that the analysis of an atomically resolved STM image on a Moiré provides the periodicity, *L*, but Ω and Φ values can only be experimentally determined in small graphene islands (images as the ones shown in Figure 1b) where atomic resolution on the substrate and layer is obtained simultaneously. Moreover, *L* and Ω may be coincident for some superstructures, only differing in the Φ, and therefore, these are usually undetectable in the STM images.

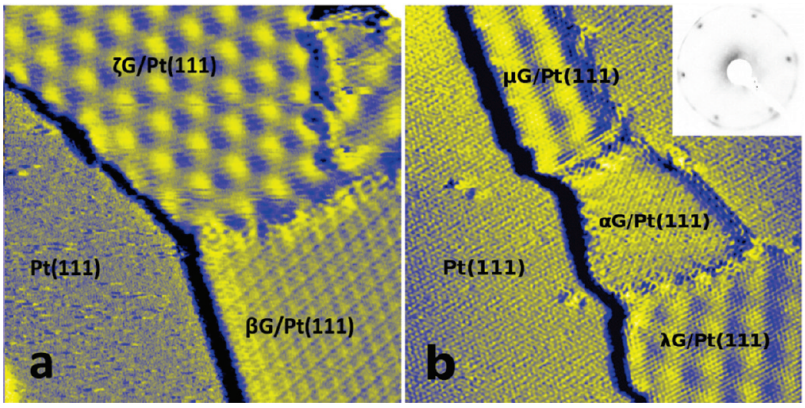

Figure 1. Constant current STM images of submonolayer graphene domains on Pt(111). Different graphene superstructures coexist together with clean Pt regions. The inset shows the characteristic ring- shaped LEED pattern of the system at 80 eV: (a) 14 × 14 nm^2, V = 100 mV, I = 2 nA; (b) 20 × 20 nm^2, V = 10 mV, I = 3.9 nA.

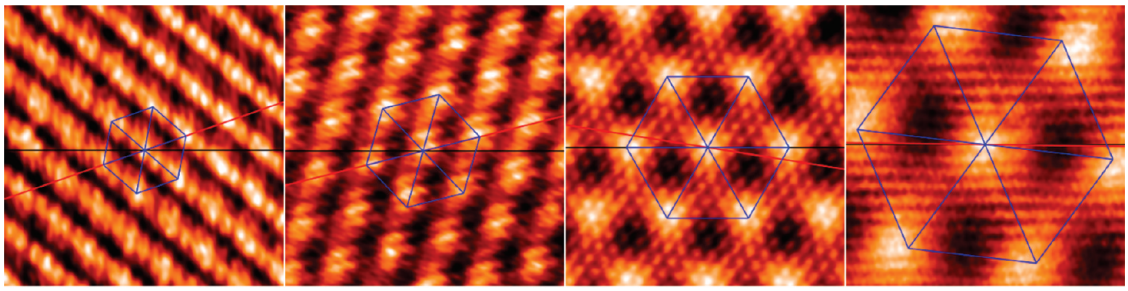

Figure 2. High resolution atomically resolved STM images of some of the periodically modulated graphene structures. The red line indicates the graphene orientation with respect to the black line, which indicates the Pt [1$\bar{1}$0] surface direction. The blue hexagon denotes the resulting Moiré structure. The structures from left to right correspond to: βG/Pt(111), γG/Pt(111), εG/Pt(111), μG/Pt(111) (this nomenclature is discussed in the text). All images are 5 × 5 nm^2. V ≈ −250, +250 mV; I ≈ 1−3 nA.

We describe the system by two overlaid hexagonal lattices corresponding to Pt (with lattice parameter a_{Pt} = 2.775 Å) and graphene (a_G = 2.46 Å). These are built from the same origin although we checked that the conclusions are independent of the considered origin. To represent graphene we used a simple hexagonal lattice instead of the honeycomb, as we are only interested in crystallographic coincidences. Nevertheless we also tried honeycomb lattice models with identical results. This counterintuitive result arises from the fact that the honeycomb lattice can also be described as two hexagonal networks shifted one from each other. As we only study crystallographic coincidences we restrain the possibility that the atom of the origin and the coincident position belong to the different hexagonal lattices of the honeycomb one. However, if we allow them, these extra coincidences gives rise to semiperiodicities, which offer no information about the real crystallography of the system, and it can be seen as another proof of the nonequivalence between the two atoms of the graphene unit cell.

Thus, we define the position of any atom in the Pt(111) surface using a single vector defined for each lattice point by two integers n and m: $\vec{a}_{Pt_{n,m}}$. Similarly, we define the vector for the graphene lattice: $\vec{a}_{gr_{i,j}}(\Phi)$. Where i and j are integer numbers and Φ is the crystallographic angle. This vector is the result of the product of a rotation matrix and the lattice vector. Now we compare both lattices by defining the mismatch, $\vec{\Delta}$:

$$|\Delta_{i,j}^{n,m}| = |\vec{a}_{Pt_{n,m}} - \vec{a}_{gr_{i,j}}(\Phi)|$$

So for every Φ and any given graphene and platinum positions the mismatch defines the difference vector between them. The aim of the model is to find for every Φ the i, j, n, and m values that minimize the modulus of Δ (see Figure 3) among all possible pairs. There usually exists a particular pair of lattice positions (ij; nm) that presents an extremely good coincidence where atomic positions almost overlap, giving a $|\Delta_{i,j}^{n,m}|$ value close to zero, and consequently they are good candidates to determine the Moiré parameters for that particular crystallographic angle. Therefore the strain of the superstructure comes, in our model, only from the strain of a single pair at the coincidence position. We applied the rotation transformation ranging from 0° to 30° with intervals of 0.05° on the graphene grid and we numerically analyzed the distances between any point in the Pt(111) lattice and any other in the graphene lattice (*i.e.*, the mismatch) searching for the smallest possible mismatch for each angle Φ. Because of the symmetry of the system, this angular range covers all the possible situations. We selected for

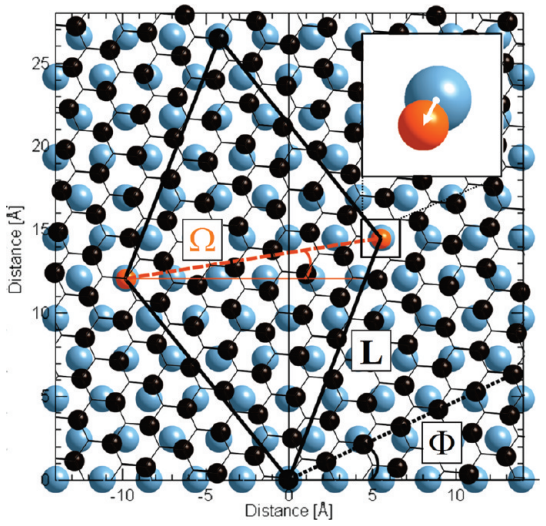

Figure 3. Diagram of the model represented for the ζG/Pt(111) superstructure. Pt atoms are represented by blue spheres, whereas the hexagonal lattice of graphene is represented by black spheres. The angle between the black dotted line and the Pt [1$\bar{1}$0] surface direction (*x* axis) represents the crystallographic angle, Φ, which is equal to 25.1° for this particular case. The orange spheres are the carbon atoms with the lowest mismatch for a given Φ, which define the Moiré unit cell indicated by the black rhombus. The angle between the orange dashed line and the Pt [1$\bar{1}$0] direction is the Moiré apparent angle (Ω). The white arrow in the inset represents the mismatch.

every Pt lattice point the corresponding closest graphene lattice position. Among these values, we searched the pairs of points with a minimum mismatch for a particular Φ angle. We found that within this angular range there is usually an angle, Φ_m, where $|\Delta_{i,j}^{n,m}|$ is at its absolute minimum and therefore at Φ_m the mismatch is the lowest

The result of this calculation is a series of parabolic-shaped curves around the Φ_m value that can be regarded as existence or stability curves. Following the upward dispersion of one of those curves, there is a point where two adjacent curves cross. On the boundaries of this angular interval the solution "jumps" to another pair of $i'j'$, $n'm'$ lattice points with a different minimum $\Phi_{m'}$ (corresponding to another parabolic curve). Figure 4a represents those stability curves, that is, the relative mismatch as a function of Φ (we define relative mismatch as the strain of the graphene unit cell: Δ/a_{gr}). As the minima of the curves correspond to the angle Φ_m where the mismatch between the coincident points is minimized, the minimum of each parabola should correspond to a superstructure, being the modulus of the associated graphene vector the periodicity of the resulting Moiré (L), showed in Figure 4b as a function of Φ. We assume that the real system tries to accommodate the graphene overlayer with an angular orientation that accumulates the smallest strain, which depends on the mismatch of the best coincident position; as a consequence only the structures at the minimum of the stability curves will be found at the surface. Because our model only takes into account the coincident positions neglecting the rest of the atoms, it suggests that the main interaction between the graphene and the substrate comes from the matching points.

We have denoted the calculated strain-mediated Moiré superstructure with Greek letters from the smallest periodicity, αG/Pt(111), to the biggest, οG/Pt(111). This model predicts the existence of 22 stable superstructures. However, only 15 of them are discernible with nonatomic resolution STM images, because for some of them, both their periodicity (*L*) and the apparent angle (Ω) are the same. All the structural parameters of the phases for the case of Pt are listed in a table in the Supporting Information. For a particular lattice position defining a Moiré, we can have two types of mismatch: Δ can be either positive or negative. In the first case, the C−C distance might try to expand in order to commensurate the surface and therefore the layer will be under tensile stress, whereas in the second case the graphene layer may tend to decrease their size leading the layer to compressive stress and introducing in the system either a reduction of the C−C bond or the emergence of out of plane configurations. We have represented in Figure 4 the domains under tensile and compressive stress using labels in blue and red color, respectively.

We have represented in Figure 4a the result of this calculation with a cutoff of the periodicity set to 23 Å since it is the largest periodicity we have found in the STM experiments. The cutoff is an important parameter in our model because it delimits the maximum radius from the origin of the model where lattice positions are taken into account, constraining the *L* of the resulting solutions.

Figure 5 shows the result of classifying all the theoretically found structures in a periodicity *versus* apparent angle plot. Every one of the 15 different superstructures of Figure 4a has been represented in the Figure 5 by a rhomboidal tick. On the same plot we have marked the different experimental Moirés found after analyzing about hundred different graphene domains. The total normalized area for every domain is represented by a 2-D Gaussian. Figure 5 shows that all the experimental determined structures can be associated to the 15 predicted ones. Interestingly, the more intense experimental points, which are proportional to their frequency of appearance, are related to the lowest values of the relative mismatch in the stability curves and therefore to the lowest strains (see table in Supporting Information).

DISCUSSION

The agreement between the experimental domains found by STM and the theoretical phases predicted with our model is very good. In fact, all the experimental phases can be related to a theoretical

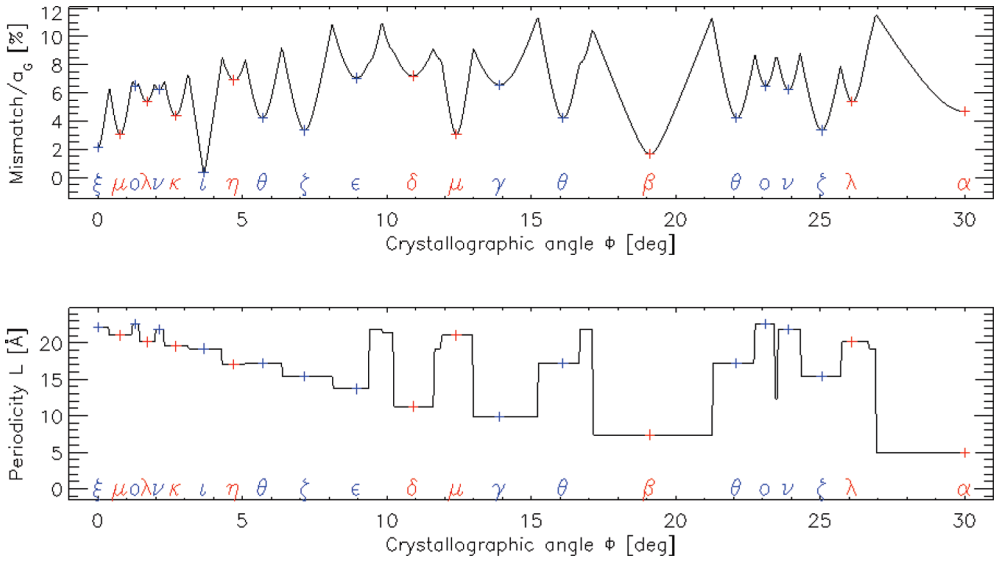

Figure 4. (Top) Relative mismatch *vs* crystallographic angle (Φ). The solid line indicates the minimum mismatch for the given angle. The blue crosses indicate the stable structures of the model with positive mismatch (tensile stress), while the red ones represent the negative mismatch (compressive stress) phases. These phases are labeled with an associated Greek letter underneath. (Bottom) Periodicity *L* *vs* crystallographic angle Φ.

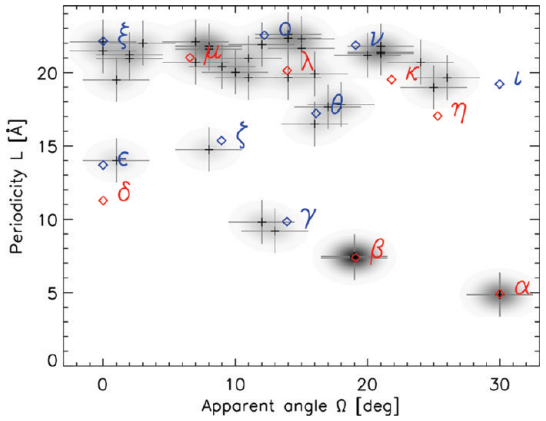

Figure 5. Periodicity *vs* apparent angle for measured STM images of graphene islands (crosses) together with the predicted Moirés (rhomboidal ticks and Greek letters). The vertical and horizontal gray lines are the error bars of the experimental determination of periodicities and Moiré angles in STM images, respectively. 2D Gaussian shapes with intensity proportional to the experimental count of finding a Moiré with a given angle and periodicity are superimposed. The interpretation of the figure can be seen as a histogram where the color intensity of a point is proportional to the occurrence of a structure.

minimum. Figure 5 shows that there only exist three exceptions that we have not found in the experimental STM sessions. The ι G/Pt(111) is in our model the structure holding the lowest mismatch (see Figure 4a). Thus, following our previous discussion it should be the most stable phase, and consequently, also the most commonly observed one. However, we have never identified it. This does not mean that it does not exist, but that its stability (evaluated by its probability of appearance) is not connected to the relative mismatch. Indeed this structure was atomically imaged by Sasaki *et al.*[20] Also, it has been recently reported at the same apparent angle the existence of a $(\sqrt{3} \times \sqrt{3})R30°$ superstructure, a particular surface reconstruction involving mass transport on the Pt surface atoms.[22] This particular reconstruction could prevent the formation of ι G/Pt(111) phase during the nucleation and growth processes.

Moreover, we have never observed the superstructures labeled as δ and η. This can be related to their high value of the mismatch (see Figure 4a), which would lead to less stable structures and therefore they would be less frequently observed. It is remarkable that both structures hold values of the relative mismatch around +7%, and therefore this could be taken as an approximative upper limit of the compressive strain that can be accommodated in the layer. We have to note that the ε phase, which presents similar mismatch but with different sign, has only been observed in samples prepared at low temperatures (950 K).

This model also predicts the formation of Moirés on other hexagonal surfaces different than Pt. We have calculated the stability curves for the hexagonal faces of Ir, Ni, Co, Cu, Pd, Rh, and Ru, finding the most stable phases according to our model correspond to the ones reported in literature (see their stability curves in Supporting Information). Thus, in Ir(111) four Moirés have been reported[8] and six superstructures were recently observed on Pd(111).[15] We have reproduced the four reported periodicities, their crystallographic and apparent angles for Ir(111) and five out of six for Pd(111). Moreover the stability curves (as the one shown in Figure 4) calculated for Ir and Pd predict superstructures holding minimum mismatch for various angles that have not been reported. We suggest that the use of polycyclic aromatic hydrocarbons as graphene precursors and low temperature annealing may lead to the formation of other unreported phases, as in the case of Pt(111).

At first glance, the domains exhibiting compressive stress shall stretch or experience out-of-plane configurations, whereas the ones submitted to tensile stress might try to enlarge the C−C bond distance. Thus, the measured corrugation for the Moirés with negative mismatch (blue labels in Figure 4) shall be exclusively correlated to electronic effects.[3] We have verified that in these cases the corrugation of the Moirés is usually smaller, and ranging from 0.2 to 0.6 Å. However the relation between the sign of the mismatch and the nature of the experimentally determined corrugation (electronic or topographic) should be treated carefully since other processes can eventually favor the emergence of topographic corrugations in the tensile-strained Moirés. Full DFT calculations for these particular structures combined with good-quality STM measurements could confirm this point.

The good agreement of our model with the experimental data for all TM suggests that the weak interaction between the Pt(111) surface and graphene is sufficient enough to force the system to accommodate into some fixed number of orientations, which minimizes the relative mismatch.[33] The existence of phases with large mismatches leads to the question of how the stress is released throughout the superstructure unit cell. It seems obvious that mismatch accumulation will lead, sooner or later, to interrupt the order of the Moiré unit cell, and therefore they would not be stable. Phases as γ would never be observed because, after a few unit cells, the coincidence structure would disrupt. However, this is not the case and for instance this particular structure is found in extended domain sizes, indicating a full release of the stress within the periodicity of the Moiré. Therefore our model confirms that the stability of the Moiré structures on TM surfaces emerges by the interplay of the local interaction between single C and TM atoms at some specific "matching-points" likely due to a favorable adsorption structure, as it has been proposed for Ru by DFT calculations.[5,6] This is the reason why our model fits better to the relative mismatch than to the total strain of the superstructure (Δ/L) and therefore, some high strained phases in the superstructure present relative high occurrence, like γ or ε phases (see Table 1 in Supporting Information).

We would like to remark that although most of the stress seems to be relaxed within the Moiré unit cell, this does not have a clear relation with the crystallographic unit cell, and some of them could be incommensurate superstructures. The analysis of the commensurability of a superstructure cannot be performed with our geometrical model. Nevertheless, the simplest explanation can be that there exists a second order (or higher) Moiré unit cell with a lower mismatch, longer periodicity, and possibly a different apparent angle. The real system would tend to relax completely inside this crystallographic supercell. Atomically resolved images of large regions of the same superstructure could confirm this point.[8]

We encourage the reader to see the stability plots for Ir(111), Pd(111), and Ni(111) as well as the table of the structural parameters of the G/Pt(111) superstructures in the Supporting Information.

CONCLUSIONS

We present a UHV-STM study of the graphene Moiré superstructures formed on Pt(111) in a multiphase preparation and a strain-based model for understanding the results. Our model is based in the search of the best coincident pair of graphene and substrate unit cell for every rotational crystallographic angle, and predicts the existence of 22 different superstructures in the case of Pt(111). Our STM measurements and previously published studies agree with our predictions. Strain minimization (creating either compressive or tensile stress) between the best coincident pairs mediates the stability of Moiré superstructures on Pt(111) and other transition metal surfaces. Thus, the stability of the Moiré structures on TM surfaces is related to a strong local interaction at the coincident lattice positions, likely due to a favorable lattice matching as it has been proposed by DFT calculations.

We also present a methodology to grow multidomain EG. The large variability of EG phases combined with the local resolution of STM can be used as a prototypical system suitable to test the fundamental concepts, as it provides a handful of Moirés and all kind of interesting features, opening unforeseen opportunities in strain- and defect-engineering on graphene. Thus, for instance, pseudomagnetic fields can be tailored with stress and domain length. These domains and superstructures can be studied by our stability curves, which predict and reproduce the existence of possible coincidence superstructures that EG can form on transition metal surfaces.

METHODS

Experiments were carried out in an ultrahigh vacuum (UHV) chamber with base pressure of 1×10^{-10} mbar. The samples were cleaned by the conventional procedure of repeated cycles of argon sputtering and annealing. The sample surface was checked by STM and LEED prior to the graphene growth. Commercial C_{60} (Sigma, 98% purity) was deposited at a rate of 0.4 monolayer per hour during 30 min, keeping the sample at room temperature (RT). The samples were then annealed by electron bombardment to temperatures up to 1200 K for 5−10 min intervals. Importantly, during this procedure the pressure never exceeded 5×10^{-10} mbar. Submonolayer coverage of flat and homogeneous graphene islands was observed on top of clean Pt regions and, thus, modifying the deposition time the total coverage can be controlled. A long deposition time leads to complete monolayer coverage.

The aim of our experimental recipe is to maximize the number of islands with different superstructures. We observed that the use of large cyclic molecules or polycyclic aromatic hydrocarbons (PAHs), in our case C_{60}, induces the formation of many different epitaxial graphitic structures. Moreover we also observed that submonolayer coverage induce the formation of smaller domains, which exhibit a larger number of different Moirés. When the coverage is close to the monolayer we observe that the graphene islands collide between them disrupting the Moirés with structural defects. We also studied the effect of the annealing temperature, which ranges between 750 and 1200 K, in order to understand the effect in the graphitization process. We observed for C_{60} that the lower the temperature is the easier it becomes to find different phases and especially the ones having periodicities between 8 and 19 Å. Therefore we conclude that the use of large PAHs in submonolayer concentrations and low temperature annealing (but above molecular dissociation temperature) induces the formation of a richer multiphase graphene.

STM images were recorded using topographic and current modes with typical biases of −250 to 250 mV and currents of 0.1−2 nA, although some images were taken with currents up to 4 nA. WSxM software was used for data acquisition and image analysis.[34] The thermal drift was corrected using a custom program in ITTVIS Interactive Data Language (IDL), in order to reduce errors in measurements of angles and distances. This program corrects the images for a given unit cell keeping the fast scan axis distances as the reference one. The error in determining the angles and periodicities is within ±2.5° and ±1.5 Å. Straight Pt steps together with atomically resolved αG/Pt(111) and βG/Pt(111) were used to calibrate the orientation of the different Moirés with respect to the Pt substrate.

Acknowledgment. We want to acknowledge financial support through the Spanish Grants: Consolider CSD2007-41; MAT2008-1497/nan, and MAT2010-17720. P.M. acknowledges financial support from the INTA program "Rafael Calvo Rodés".

Supporting Information Available: Previous studies reproduced by our model; experimental *vs* model results; additional figures and tables. This material is available free of charge *via* the Internet at http://pubs.acs.org.

REFERENCES AND NOTES

1. Wintterlin, J.; Bocquet, M.-L. Graphene on Metal Surfaces. *Surf. Sci.* **2009**, *603*, 1841–1852.
2. Martoccia, D.; Willmott, P. R.; Brugger, T.; Björck, M.; Günther, S.; Schlepütz, C. M.; Cervellino, A.; Pauli, S. A.; Patterson, B. D.; Marchini, S.; *et al.* Graphene on Ru(0001): A 25 × 25 Supercell. *Phys. Rev. Lett.* **2008**, *101*, 126102.
3. Vázquez de Parga, A. L.; Calleja, F.; Borca, B.; Passeggi, M. C. G., Jr.; Hinarejos, J. J.; Guinea, F.; Miranda, R. Periodically Rippled Graphene: Growth and Spatially Resolved Electronic Structure. *Phys. Rev. Lett.* **2008**, *100*, 056807.
4. Marchini, S.; Günther, S.; Wintterlin, J. Scanning Tunneling Microscopy of Graphene on Ru(0001). *Phys. Rev. B* **2007**, *76*, 075429.
5. Moritz, W.; Wang, B.; Bocquet, M. -L.; Brugger, T.; Greber, T.; Wintterlin, J.; Gunther, S. Structure Determinaton of the Coincidence Phase of Graphene on Ru(0001). *Phys. Rev. Lett.* **2010**, *104*, 136102.
6. Jiang, D.; Du, M.-H.; Dai, S. First Principles Study of the Graphene/Ru(0001) Interface. *J. Chem. Phys.* **2009**, *130*, 074705.
7. Coraux, J.; ŃDiaye, A. T.; Busse, C.; Michely, T. Stuctural Coherency of Graphene on Ir(111). *Nano Lett.* **2008**, *8*, 565–570.
8. Loginova, E.; Nie, S.; Thürmer, K.; Bartelt, N. C.; McCarty, K. F. Defects of Graphene on Ir(111): Rotational Domains and Ridges. *Phys. Rev. B* **2009**, *80*, 085430.
9. Wang, B.; Caffio, M.; Bromley, C.; Früchtl, H.; Schaub, R. Coupling Epitaxy, Chemical Bonding, and Work Function at the Local Scale in Transition Metal-Supported Graphene. *ACS Nano* **2010**, *4*, 5773–5782.
10. Land, T. A.; Michely, T.; Behm, R. J.; Hemminger, J. C.; Comsa, G. STM Investigation of Single Layer Graphite Structures Produced on Pt(111) by Hydrocarbon Decomposition. *Surf. Sci.* **1992**, *264*, 261–270.
11. Sutter, P.; Sadowski, J. T.; Sutter, E. Graphene on Pt(111): Growth and Substrate Interaction. *Phys. Rev. B* **2009**, *80*, 245411.
12. Gao, M.; Pan, Y.; Huang, L.; Hu, H.; Zhang, L. Z.; Guo, H. M.; Du, S. X.; Gao, H.-J. Epitaxial Growth and Structural property of Graphene on Pt(111). *App. Phys. Lett.* **2011**, *98*, 033101.
13. Gao, L; Guest, J. R.; Guisinger, N. P. Epitaxial Graphene on Cu(111). *Nano Lett.* **2010**, *10*, 3512–3516.
14. Kwon, S.-Y.; Ciobanu, C. V.; Petrova, V.; Shenoy, V. B.; Vivek, B. S.; Bareño, J.; Gambin, V.; Petrov, I.; Kodambaka, S. Growth of Semiconducting Graphene on Palladium. *Nano Lett.* **2009**, *9*, 3985–3990.
15. Murata, Y.; Starodub, E.; Kappes, B. B.; Ciobanu, C. V.; Bartelt, N. C.; McCarthy, K. F.; Kodambaka, S. Orientation-Dependent Work Function of Graphene on Pd(111). *App. Phys. Lett.* **2010**, *97*, 143114.
16. Eom, D.; Prezzi, D.; Rim, K. T.; Zhou, H.; Lefenfeld, M.; Xiao, S.; Nuckolls, C.; Hybertsen, M. S.; Heinz, T. F.; Flynn, G. W. Structure and Electronic Properties of Graphene Nanoislands on Co(0001). *Nano Lett.* **2009**, *9*, 2844–2848.
17. Murata, Y.; Petrova, V.; Kappes, B. B.; Ebnonnasir, A.; Petrov, I.; Xie, Y.-H.; Ciobanu, C. V.; Kodambaka, S. Moiré Superstructures of Graphene on Faceted Nickel Islands. *ACS Nano* **2010**, *11*, 6509–6514.
18. Enachescu, M.; Schleef, D.; Ogletree, D. F.; Salmeron, M. Integration of Point-Contact Microscopy and Atomic-Force Microscopy: Application to Characterization of Graphite/Pt(111). *Phys. Rev. B* **1999**, *60*, 16913.
19. Fujita, T.; Kobayashi, W.; Oshima, C. Novel Structures of Carbon Layers on a Pt(111) Surface. *Surf. Interface Anal.* **2005**, *37*, 120–123.
20. Sasaki, M.; Yamada, Y.; Ogiwara, Y.; Yagyu, S.; Yamamoto, S. Moiré Contrast in the Local Tunneling Barrier Height Images of Monolayer Graphite on Pt(111). *Phys. Rev. B* **2000**, *61*, 015653.
21. Ueta, H.; Saida, M.; Nakai, C.; Yamada, Y.; Sasaki, M.; Yamamoto, S. Highly Oriented Monolayer Graphite Formation on Pt(111) by a Supersonic Methane Beam. *Surf. Sci.* **2004**, *560*, 183–190.
22. Otero, G.; Gonzalez, C.; Pinardi, A. L.; Merino, P.; Gardonio, S.; Lizzit, S.; Blanco-Rey, M.; Van de Ruit, K.; Flipse, C. F. J.; Méndez, J.; *et al.* Ordered Vacancy Network Induced by the Growth of Epitaxial Graphene on Pt(111). *Phys. Rev. Lett.* **2010**, *105*, 216102.
23. Lahiri, J.; Lin, Y.; Bozkurt, P.; Oleynik, I. I.; Batzill, M. An Extended Defect in Graphene as a Metallic Wire. *Nat. Nanotechnol.* **2010**, *5*, 326–329.
24. Ugeda, M. M.; Brihuega, I.; Guinea, F.; Gómez-Rodríguez, J. M. Missing Atom as a Source of Carbon Magnetism. *Phys. Rev. Lett.* **2010**, *104*, 096804.
25. Banhart, F.; Kotakoski, J.; Krasheninnikov, A. V. Structural Defects in Graphene. *ACS Nano* **2011**, *5*, 26–41.
26. Yazyev, O. V.; Louie, S. G. Electronic Transport in Polycrystalline Graphene. *Nat. Mater.* **2010**, *9*, 806–809.
27. Kim, K.; Lee, Z.; Regan, W.; Kisielowski, C.; Crommie, M. F.; Zettl, A. Grain Boundary Mapping in Polycrystalline Graphene. *ACS Nano* **2011**, *5*, 2142–2146.
28. Huang, P. Y.; Ruiz-Vargas, C. S.; van der Zande, A. M.; Whitney, W. S.; Levendorf, M. P.; Kevek, J. W.; Garg, S.; Alden, J. S.; Hustedt, C. J.; Zhu, Y.; *et al.* Grains and Grain Boundaries in Single-Layer Graphene Atomic Patchwork Quilts. *Nature* **2011**, *469*, 389–392.
29. Guinea, F.; Katsnelson, M. I.; Geim, A. K. Energy Gaps and a Zero-Field Quantum Hall Effect in Graphene by Strain Engineering. *Nat. Phys.* **2009**, *6*, 30–33.
30. Levy, N.; Burke, S. A.; Meaker, K. L.; Panlasigui, M.; Zettl, A.; Guinea, F.; Castro Neto, A. H.; Crommie, M. F. Stain-Induced Pseudomagnetic Fields Greater than 300 T in Graphene Nanobubbles. *Science* **2010**, *329*, 544–547.
31. Wassman, T.; Seitsonen, A. P.; Saitta, A. M.; Lazzeri, M.; Mauri, F. Clar's Theory, π-Electron Distribution, and

Geometry of Graphene Nanoribbons. *J. Am. Chem. Soc.* **2010**, *132*, 3440–3451.
32. Cai, J.; Ruffieux, P.; Jaafar, R.; Bieri, M.; Braun, T.; Blankenburg, S.; Muoth, M.; Seitsonen, A. P.; Saleh, M.; Feng, X.; Müllen, K.; Fasel, R. Atomically Precise Bottom-Up Fabrication of Graphene Nanoribbons. *Nature* **2010**, *466*, 470–473.
33. Preobrajenski, A. B.; Ng, M. L.; Vinogradov, A. S.; Martensson, N. Controlling Graphene Corrugation on Lattice-Mismatched Substrates. *Phys. Rev. B* **2008**, *78*, 073401.
34. Horcas, I.; Fernández, R.; Gómez-Ródriguez, J. M.; Colchero, J.; Gómez-Herrero, J.; Baró, A. M.; WSXM, A Software for Scanning Probe Microscopy and a Tool for Nanotechnology. *Rev. Sci. Instrum.* **2007**, *78*, 013705.